

A NO_x diagnostic system based on a spectral ultraviolet/visible imaging device

M. Ruão, M. Costa*, M.G. Carvalho

Mechanical Engineering Department, Instituto Superior Técnico/Technical University of Lisbon, Av. Rovisco Pais, 1049-001 Lisbon, Portugal

Received 9 November 1998; accepted 17 February 1999

Abstract

The present investigation is aimed to develop and test a NO_x diagnostic system based on a spectral ultraviolet/visible imaging device. The study was performed in a small-scale laboratory furnace fired by a propane or ethylene swirl burner. The data reported include flue-gas concentrations of O₂, CO₂, CO, unburnt hydrocarbons and NO_x, obtained with conventional techniques, and photometric data of spontaneous emission of OH and CH radicals, obtained with the imaging device, from various regions of the flame. All these measurements have been obtained for twenty three furnace operating conditions which quantify the effects of the gaseous fuel (propane and ethylene), flue-gas recirculation, heat losses through the furnace walls to the surroundings and excess air. Against this background, it was possible to obtain a wide range of NO_x emissions. In addition, the analysis of detailed near burner in-flame data of local mean major gas-phase species and gas temperatures collected for four furnace operating conditions has indicated that NO_x formation was strongly dominated by the prompt (or Fenimore) mechanism. The results reveal that there is an excellent correlation between the NO_x emissions from propane or ethylene flames and the OH + CH photometric data, which can be mathematically expressed as a logarithmic function, provided that the radicals images are collected from a flame zone close to the burner exit. © 1999 Elsevier Science Ltd. All rights reserved.

Keywords: Propane; Ethylene; Nitrogen oxides; Diagnostic system; Spectral ultraviolet/visible imaging device

1. Introduction

Spectral studies in the ultraviolet (UV) and visible ranges yield detailed information of combustion processes and have been the subject of recent investigations, not only in internal combustion engines [1–3] but also in industrial combustion systems [4,5]. When using the flue-gas composition as the input value for a closed-loop control, the time scale for the control system becomes much longer than the combustion time scales [4]. The present investigation aims to develop and test a NO_x diagnostic system based on a spectral ultraviolet/visible imaging device which will allow a faster response.

The tests were performed in a small-scale laboratory furnace. Conventional techniques were used to gather flue-gas and in-flame data for several furnace operating conditions, which combined the use of two gaseous fuels (propane and ethylene), flue-gas recirculation (FGR), furnace walls with and without insulation and two excess air levels. In this way, it was possible to obtain for the

present combustion system a wide range of NO_x emissions. Simultaneously, a spectral ultraviolet/visible imaging device was used to detect OH and CH spontaneous emissions from various flame zones for all the conditions studied with conventional techniques. The NO_x emission data were then confronted against the photometric data to establish a correlation between the NO_x flue-gas concentrations and both the OH and CH spontaneous emission.

2. Indicator radicals for NO_x formation in gas flames

In the combustion of fuels not containing nitrogen compounds, NO_x is formed through the thermal and prompt (or Fenimore) mechanisms. The formation of thermal-NO_x takes place through the extended Zel'dovich mechanism [6]:



with reaction (1) controlling the NO_x formation. In addition,

* Corresponding author. Tel.: + 351-1-8417186; fax: + 351-1-8475545.

E-mail address: mcosta@navier.ist.utl.pt (M. Costa)

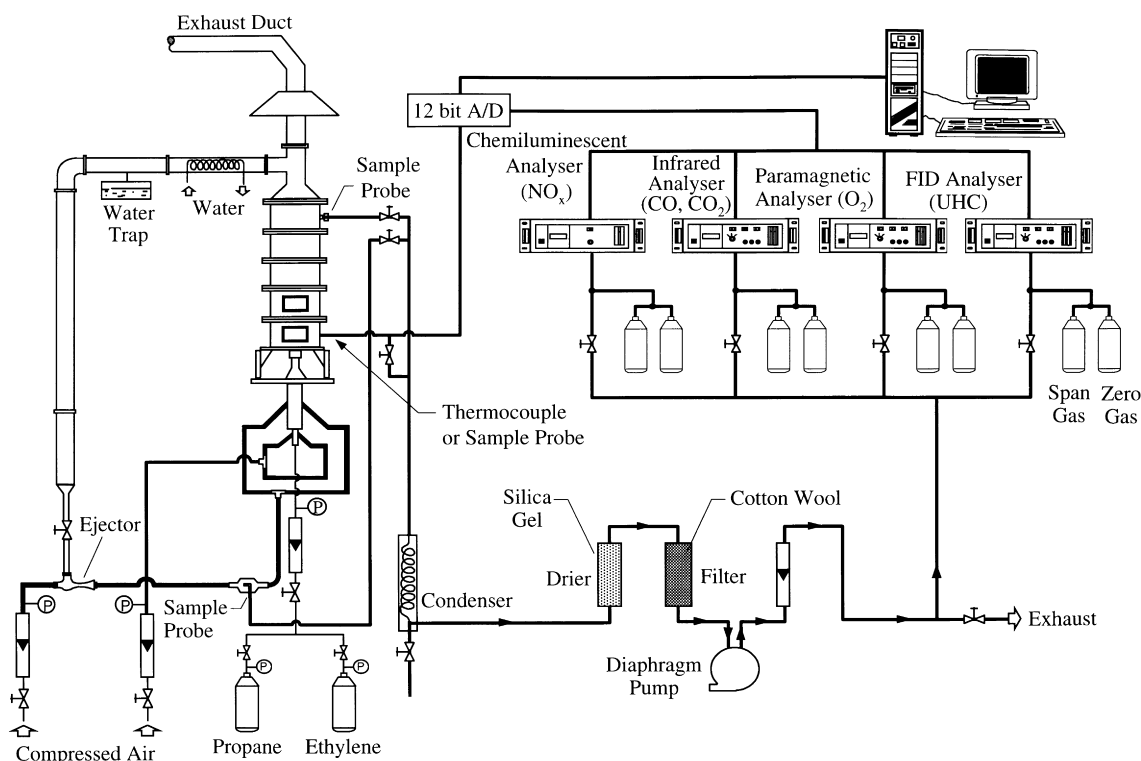


Fig. 1. Schematic of the furnace and measurement equipment.

because reaction (1) is strongly temperature dependent due to its high activation energy, thermal- NO_x formation is significant only at high temperatures.

Prompt- NO_x in hydrocarbon flames is formed primarily by a reaction sequence described by Miller and Bowman [7] as follows:



Note that the last reaction in both NO_x mechanisms (reactions (3) and (3a)) is the same.

Owing to the impossibility to detect spontaneous NO emission in flames of fuels not containing nitrogen compounds, there is a need to find indicators for its formation in such flames. In the case of the Zel'dovich mechanism the radical OH is the only possible NO indicator based on spontaneous emission. The prompt mechanism is initiated through reaction (4) which involves the radical CH . It is obvious to take its spontaneous emission as a possible prompt- NO_x indicator. Other possible indicator of the prompt mechanism is the radical OH , reaction (3), in common with the thermal mechanism. Let us then assume

that the spontaneous emission of the radical OH and of both the radicals OH and CH are linked, in same way, to the NO_x formation via the thermal and prompt mechanisms, respectively.

3. The experimental facility

A schematic of the experimental facility is shown in Fig. 1. It comprises a small-scale laboratory furnace up-fired by a swirl burner equipped with facilities for flue-gas recycling. The combustion chamber is cylindrical in shape and consists of five interchangeable steel segments each 0.2 m in height and 0.3 m in internal diameter. Each segment can be insulated using a ceramic fibre blanket. Each one of the two lower segments has four rectangular ports for probing and/or optical access which are closed with quartz or steel inserts. The burner geometry, shown in Fig. 2, consists of a burner gun (i.d. 8 mm, o.d. 12 mm) and an air supply in a conventional concentric configuration. The latter has two separated air streams, both having very thin guide vanes for inducing swirl. In the present work, the inner and outer streams were fitted with guide vanes of constant cord and angle of 60 and 30°, respectively.

Before entering the burner, the air flows through an ejector in order to suck flue-gas directly from the exhaust duct of the furnace as illustrated in Fig. 1. The remainder of the flue-gas is exhausted from the test furnace. The flue-gas withdrawn for recirculation purposes is controlled by a valve and

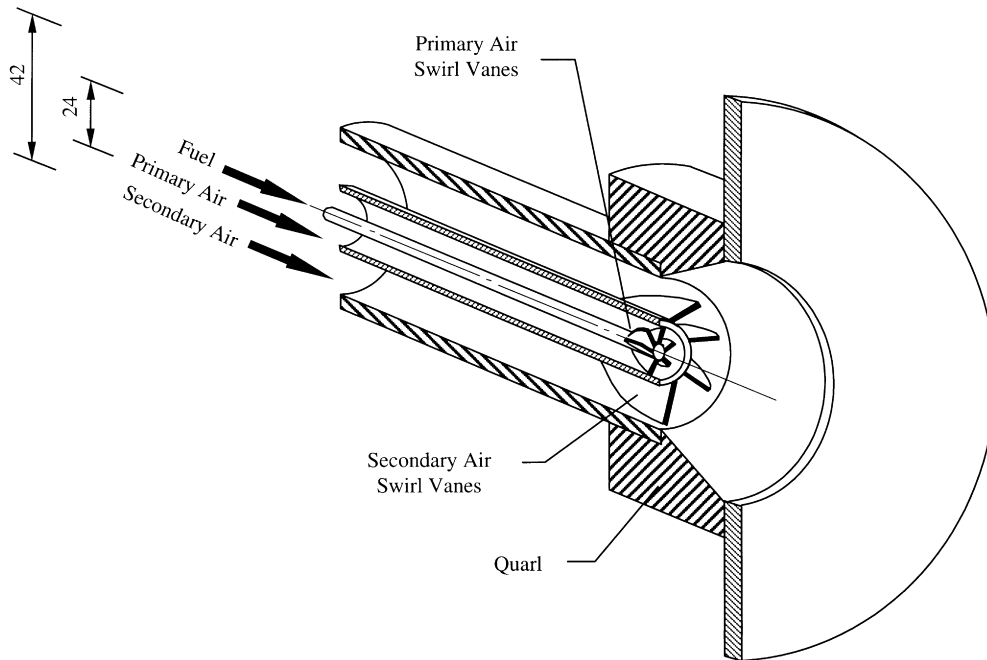


Fig. 2. Schematic of the burner arrangement.

cooled by a water coil placed in the recycling duct after which the condensate is removed. The oxidant mixture (fresh air + flue-gas) is then directed to the burner. A probe is permanently placed just before the burner to measure the oxidant composition so that recirculation rates can be calculated.

4. Experimental method

4.1. Flue-gas measurements

The sampling of flue-gas for the measurement of O_2 , CO_2 , CO , unburnt hydrocarbons (UHC) and NO_x concentrations was achieved using an aerodynamically quenched quartz probe. The probe design and dimensions were similar to those used by Drake et al. [8]. The probe was mounted on a traverse mechanism which enabled radial movement across the entire furnace at the exit sampling location ($x/D = 23.8$ — x is the axial distance from the quarl exit plane and D is the inner diameter of the secondary air tube).

A schematic of the gas analysis system is also shown in Fig. 1. The gas sample was drawn through the probe and the sampling system by an oil-free diaphragm pump. A condenser removed the main particulate burden and condensate. A drier and a filter removed any residual moisture and particles so that a constant supply of clean dry combustion gases was delivered to each instrument through a manifold to give species concentrations on a dry basis. The analytical instrumentation included a magnetic pressure analyser for O_2 measurements, non-dispersive infrared gas analysers for CO_2 and CO , a flame ionisation detector for UHC measure-

ments and a chemiluminescent analyser for NO_x measurements. Zero and span calibrations with standard mixtures were performed before and after each measurement session. The maximum drift in the calibration was within $\pm 2\%$ of the full scale.

At the furnace exit, radial profiles showed that the concentration of the species were uniform so that probe effects were likely to be negligible and errors arose mainly from quenching of chemical reactions, sample handling and analysis. Adequate quenching of the chemical reactions was achieved and NO_2 removal by acid formation within the probe and sampling system was negligible. Repeatability of the data was, on average, within 5%.

4.2. In-flame measurements

Concentration measurements of O_2 , CO_2 , CO , UHC and NO_x in the near burner region were made on a dry basis as described earlier. However, a water-cooled probe was used instead of the quartz probe. It comprised a centrally located 2 mm i.d. tube through which quenched samples were evacuated, surrounded by two concentric tubes for probe cooling. In the near burner region the major sources of uncertainties were associated with the quenching of chemical reactions and aerodynamic disturbance of the flow. Quenching of the chemical reactions was rapidly achieved upon the samples being drawn into the central tube of the probe because of the high water cooling rate in its surrounding annulus—our best estimate indicated quenching rates of about 10^6 K/sec. As in flue-gas measurements, uncertainty because of NO_2 removal by acid formation within the probe and sampling system was negligible. No attempt was made

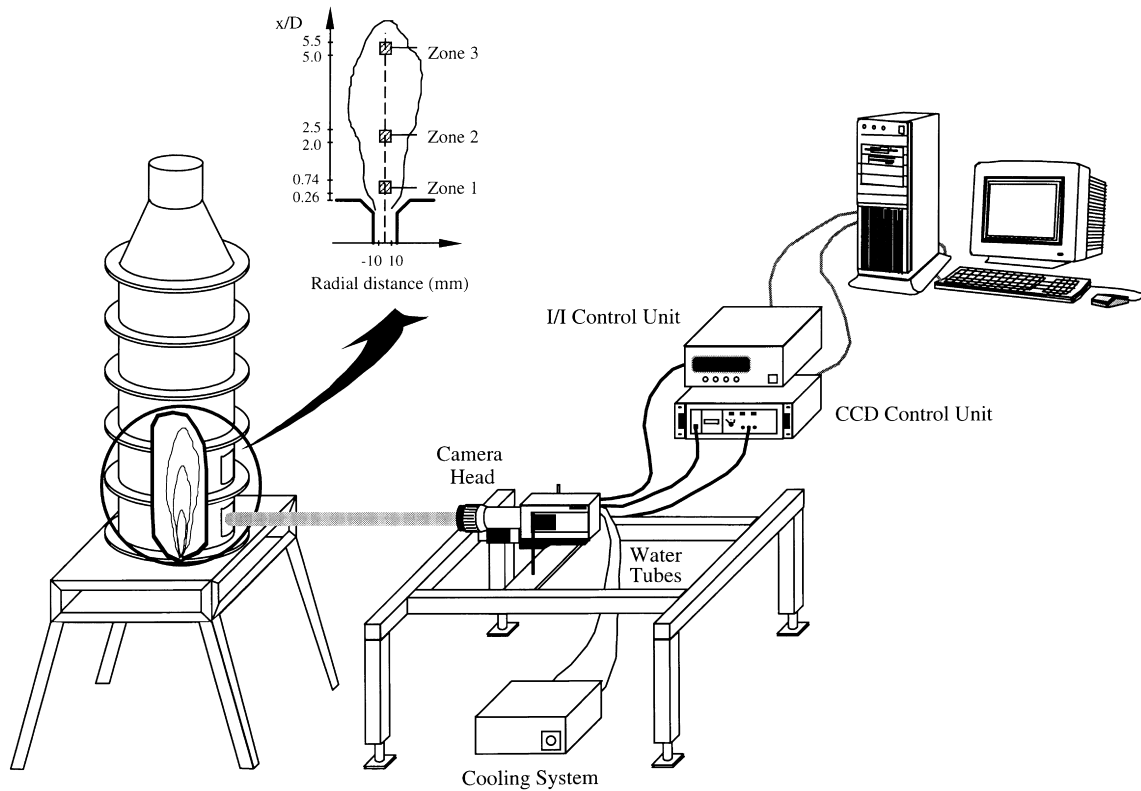


Fig. 3. Schematic of the imaging device.

to quantify the probe flow disturbances. The repeatability of the data was, on an average, within 10%.

Gas temperature measurements were obtained using uncoated 25 μm diameter Pt/Pt:13% Rh thermocouples. The hot junction was installed and supported on 300 μm wires of the same material as that of the junction. The

300 μm wires were located in a twin-bore alumina sheath with an external diameter of 4 mm and placed inside a stainless steel tube. As flame stabilisation on the probe was not observed, interference effects were unlikely to have been important and, hence, no effort was made to quantify them. Radiation losses represent the major source of

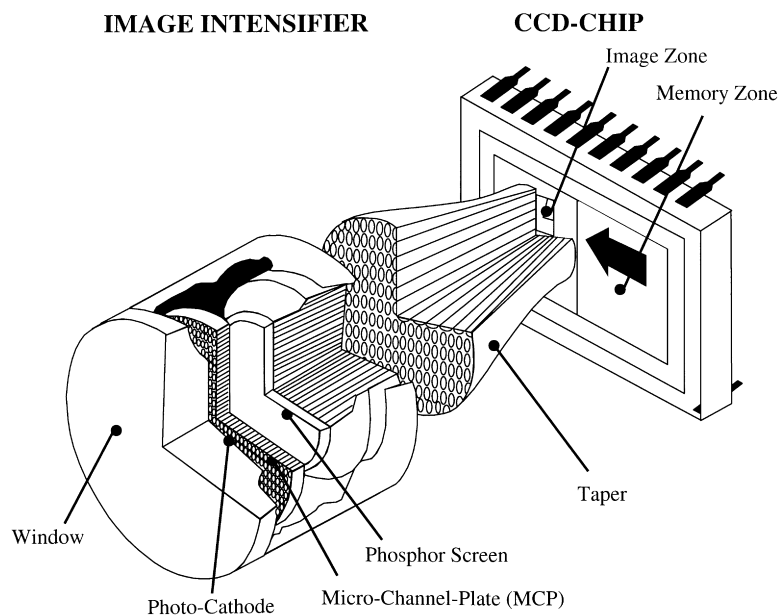
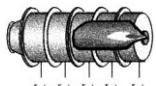
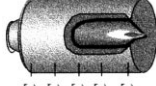
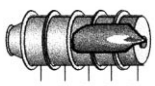
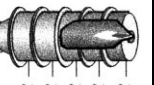


Fig. 4. Overview of the intensifier/taper/CCD-sensor configuration.

Table 1
Furnace operating conditions and flue-gas data

Group	Flame	Fuel	Temperature of the furnace walls for R = 0%	Oxidant (dry volume)		λ	R (%)	Flue-gas composition (dry volume)				
				O ₂ (%)	CO ₂ (%)			O ₂ (%)	CO ₂ (%)	CO (ppm)	UHC (ppm)	NO _x (ppm, 3% exc. O ₂)
I	P1	Propane (C ₃ H ₈)	 180°C	20.9	0.0	1.07	0.0	1.4	12.6	236	21.5	32.0
	P2		20.3	0.3	2.9		1.4	12.5	285	11.1	29.4	
	P3		18.4	1.5	14.3		1.3	12.7	97	16.1	20.2	
	P4		17.7	1.9	18.9		1.3	12.7	123	15.8	17.8	
	P5		17.2	2.3	24.1		1.4	12.6	430	29.0	14.0	
II	P6	Propane (C ₃ H ₈)	 670°C	20.9	0.0	1.07	0.0	1.4	12.9	71	1.0	49.2
	P7		19.5	0.7	7.4		1.3	13.1	38	0.7	42.4	
	P8		17.6	2.1	20.2		1.5	12.8	54	0.5	33.3	
	P9		16.8	2.5	26.4		1.5	12.9	65	0	27.1	
	P10		16.2	3.0	31.4		1.5	12.6	43	0	18.6	
	P11		15.6	3.1	36.8		1.5	12.7	16	0	16.3	
	P12		14.7	3.8	44.5		1.3	13.1	0	0	8.8	
III	E1	Ethylene (C ₂ H ₄)	 190°C	20.9	0.0	1.15	0.0	2.9	12.7	0	1.5	61.8
	E2		18.6	1.5	14.9		3.5	12.4	0	0.5	58.0	
	E3		17.2	2.9	26.3		3.2	12.6	0	0	41.9	
	E4		16.4	3.1	33.8		3.2	12.6	0	0	32.1	
	E5		15.6	3.7	42.6		3.2	12.6	0	6.5	24.0	
IV	P13	Propane (C ₃ H ₈)	 185°C	20.9	0.0	1.15	0.0	3.0	12.1	0	0	44.2
	P14		20.2	0.5	4.1		3.0	12.0	0	0	37.3	
	P15		19.2	1.1	10.3		2.9	12.1	0	0	29.8	
	P16		18.5	1.4	15.3		3.1	11.9	0	0	29.3	
	P17		17.5	2.1	22.9		2.9	12.1	0	0	21.6	
P18	16.8	2.8	29.0	2.8	11.9	0	5.2	17.1				

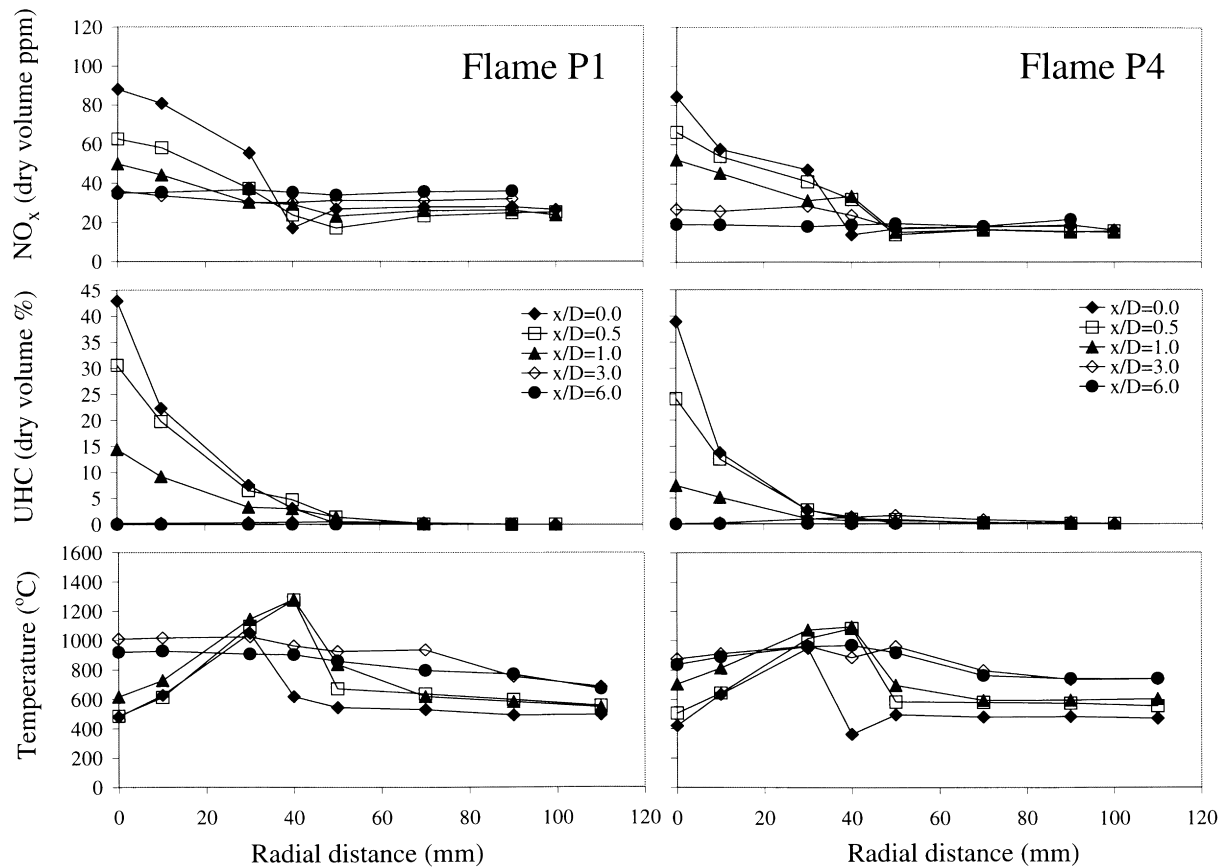


Fig. 5. Radial profiles of local mean concentrations of NO_x and UHC and gas temperatures for flames P1 and P4.

uncertainty in the mean temperature measurements. An attempt made to quantify them on the basis of a theoretical expression developed by De [9] led to uncertainties of about 5% in the regions of highest temperatures and lower elsewhere.

Both probes were mounted on a 3-D computer controlled traverse mechanism which allowed for axial and radial movements throughout the furnace. The analogue output of the analysers and of the thermocouple were transmitted via A/D boards to a computer where the signals were processed and the mean values computed. No thermal distortion of the probes was observed and the positioning of the probes in the furnace was accurate to within ± 0.5 mm.

4.3. Images acquisition

The images were acquired using an intensified CCD camera system [10], equipped with an UV objective (UV Nikon, 105 mm, $f/4.5$). Fig. 3 shows a schematic of the imaging device arrangement. The camera consists of an image intensifier that is optically coupled via a fibre optic imaging bundle (taper) to a CCD chip whose configuration is shown in Fig. 4. The incident light on the photo cathode, which has sufficient spectral sensitivity in a wide

wavelength range from 200 to 900 nm, causes emission of electrons proportional to the number of incident photons. These photoelectrons are accelerated by a strong electric field from the cathode to the micro-channel-plate (MCP), where the electron current is intensified by a secondary electrons emission in the channels of the plate, maintaining the spatial resolution. The gain depends on this voltage across the MCP and both the gain and gating time were kept constant throughout the present study for the purpose of contrasting the data. The electron stream is accelerated again between the MCP and the phosphor screen before hitting the phosphor screen, resulting in the emission of visible light. The coupling of the image intensifier and CCD chip is made via a taper, which has a much higher transmission when compared to a lens coupling. The CCD chip (TH7863, Thomson) has 576×384 (horizontal \times vertical) pixels and is divided into two identical arrays. The upper part of the chip is the image zone, which receives the optical information, and the lower half is the memory zone, into which the image field is transferred for subsequent read out by an 12-bit A/D-converter and stored under software control within the RAM of the computer. The CCD chip is cooled by a Peltier element at 10°C to minimise thermal dark current.

To eliminate the dark signal in the present investigation,

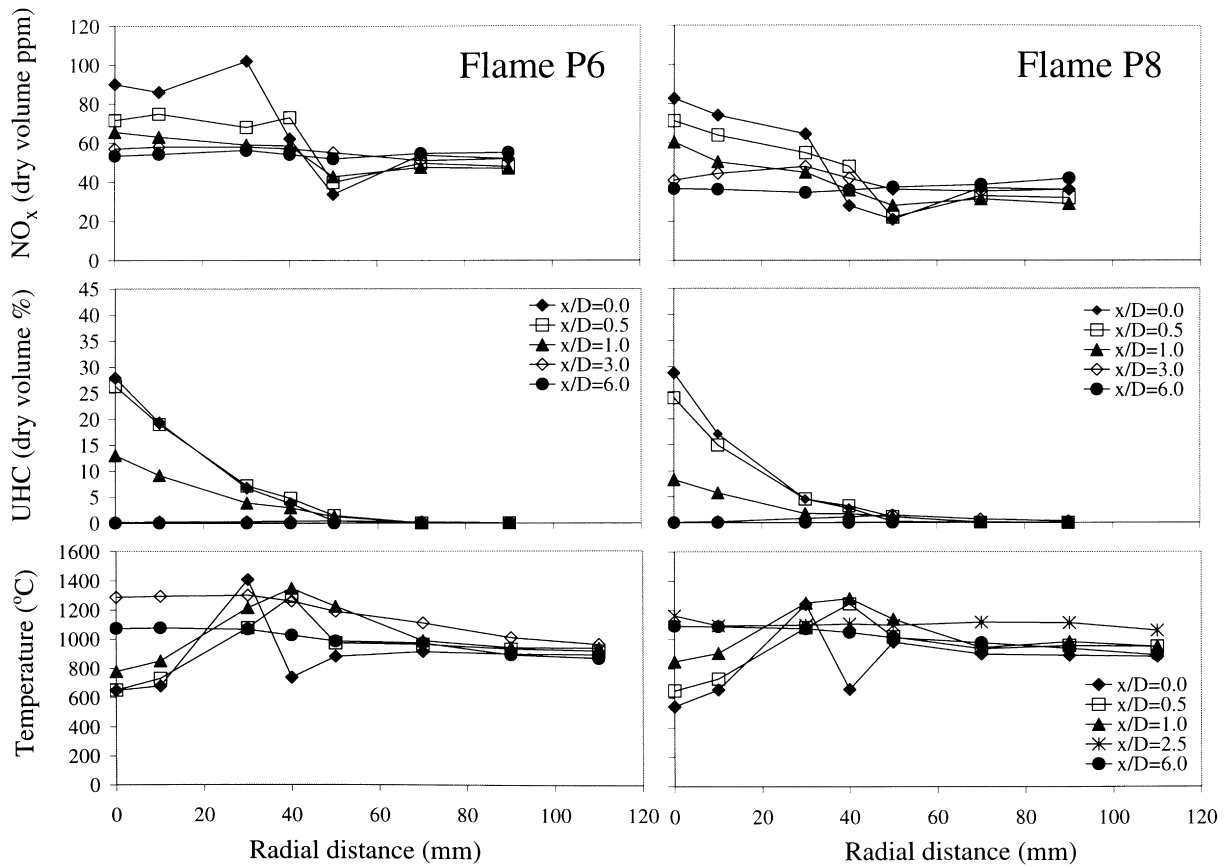


Fig. 6. Radial profiles of local mean concentrations of NO_x and UHC and gas temperatures for flames P6 and P8.

background images were taken with capped camera, under the same integration time and gain of the measured images, for subsequent subtraction from the original measured images. The OH radical was detected using a UG11 glass filter and the CH radical was filtered using a band pass filter centred at 431 nm with a bandwidth of 10.3 nm. All the photometric images of OH and CH radicals were averaged over 30 times to provide statistical mean. For the calibration

of the spatial resolution, a paper map was placed in the centre of the furnace and images of the map were taken at three different zones, which are shown in Fig. 3. Each image obtained, which maintains the spatial resolution, showed an area of 20 mm × 20 mm. The attenuation of the intensity due to soot deposition on the optical access of the furnace was also taken into account. To this end, an image of a tungsten lamp placed in the centre of the furnace was

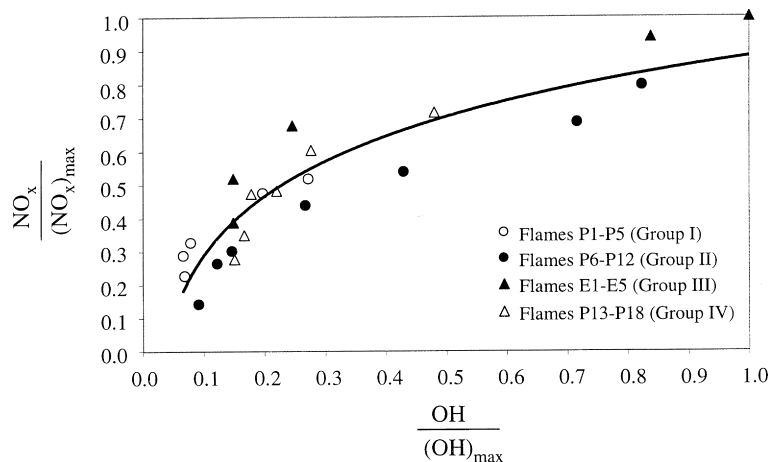


Fig. 7. Variation of the NO_x emission, normalised by its maximum, with the OH intensity, normalised by its maximum value.

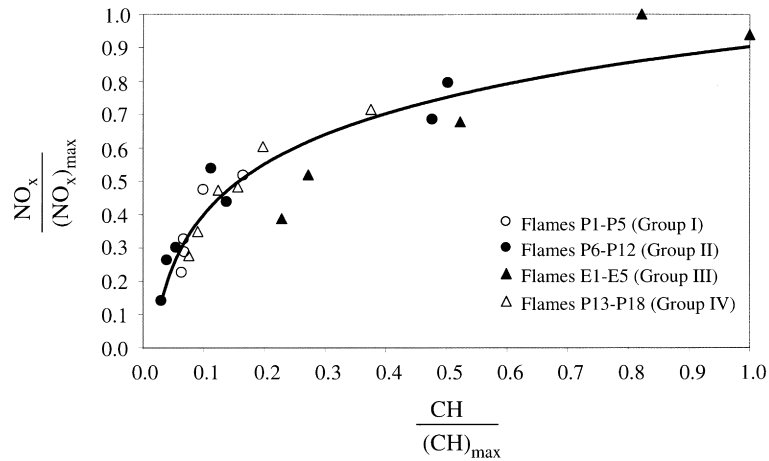


Fig. 8. Variation of the NO_x emission, normalised by its maximum, with the CH intensity, normalised by its maximum value.

taken before and after every measurement to quantify the change in the transmissivity of the quartz window. The maximum correction associated with the intensity attenuation occurred in zone 1 (see Fig. 3): 2.5% in the case of the CH for the ethylene flames.

To take into account the soot continuous radiation, the flame temperature was estimated by the two-colour pyrometry method [11,12]. The correct temperature can only be measured when band spectra do not exist in the measured wavelengths. For this purpose, we have used two filters centred at 530 and 660 nm with a bandwidth of approximately 8 nm and assumed that the spectral emissivity of the flame is the same at the two wavelengths. The entire system was calibrated by means of a black-body furnace which could operate in the range 300–1500°C. For each flame, images with the 660 nm filter were collected and knowing that OH-radical has its main head at 306 nm and CH at 431 nm [13], we used the calibration curves I_{306}/I_{660} and I_{431}/I_{660} , where I_λ is the luminous intensity obtained using a filter centred at λ , to subtract the soot radiation to the OH and CH band emission. The maximum soot background correction occurred in zone 1

(see Fig. 3): 1.5% in the case of the CH for the ethylene flames.

Our best estimated indicated uncertainties of less than 5%, considering the uncertainties of the tungsten lamp, the transmissivity change of the optical access and the soot continuous radiation correction. Repeatability of the photometric data was, on average, within 5%.

5. Test conditions

The furnace operating conditions are summarised in Table 1 and encompass twenty three experimental flames. It should be noted that the present investigation has involved four different groups of flames, corresponding to two gaseous fuels (propane and ethylene), furnace combustion chamber walls with and without insulation and two excess air coefficients ($\lambda = 1.07$ and 1.15). In all the tests performed, the primary air flow was about 20% of the total air flow. The thermal input (≈ 15 kW) was kept constant for all flames studied and for each group of them the fresh air flow rate was held constant being the flue-gas

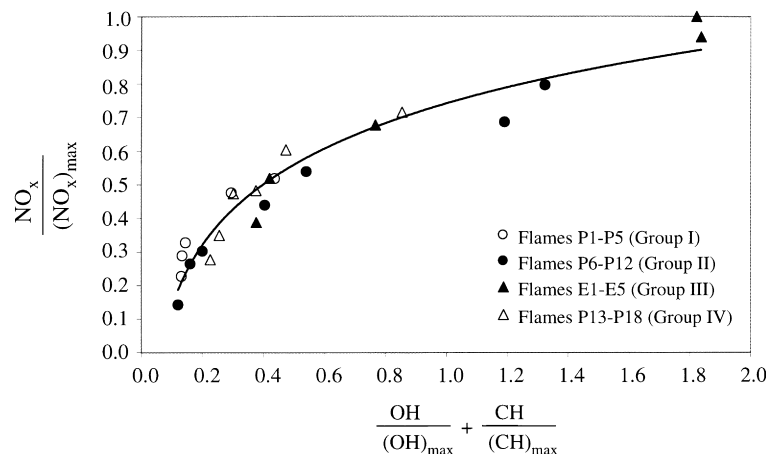


Fig. 9. Variation of the NO_x emission, normalised by its maximum, with the OH + CH intensity, each normalised by its maximum value.

flow rate gradually increased. In this work the FGR rate is defined as [14]:

$$R = \frac{\dot{m}_{\text{rec}}}{\dot{m}_a + \dot{m}_f} \times 100, \quad (8)$$

where \dot{m}_{rec} is the mass flow of recycled flue-gas products per unit time.

6. Results and discussion

6.1. The relative importance of the prompt and thermal mechanisms in the present flames

Table 1 lists the furnace operating conditions used in the present work along with flue-gas data revealing a wide range of NO_x emissions, as initially intended. Note that the values of the NO_x emissions given in the table have been reduced to 3% of O_2 in the combustion products. The effects of the gaseous fuel and FGR on pollutants emissions are fully discussed elsewhere [15,16]. In addition to the wide range of NO_x emissions required, it is important to examine, at least qualitatively, the sources of NO_x formation (prompt and/or thermal) from the present flames in order to investigate the relative importance of reactions (3), (3a) and (4). To this end we have conducted detailed near burner in-flame measurements for four furnace operating conditions: flames P1 and P4 of group I and flames P6 and P8 of group II (see Table 1).

Fig. 5 shows radial profiles of local mean concentrations of NO_x , UHC and gas temperatures for flames P1 and P4 at five axial locations. For both flames it can be observed that the NO_x concentration maxima occur in their central region close to the burner quartz exit (axial locations of $x/D = 0$ and 0.5). In this region, the high UHC concentrations and the relatively low gas temperatures measured clearly indicate that the prompt mechanism is the dominant source of NO_x in both flames. Further, because thermal- NO_x formation is strongly temperature dependent, as mentioned earlier, thermal- NO_x is significant only at temperatures greater than 1500°C [17]. The maximum temperatures measured for flames P1 and P4 barely exceed 1200 and 1000°C , respectively. Owing to turbulent fluctuations the instantaneous temperature may be sufficiently high to promote thermal- NO_x formation, but the value of the maximum mean temperature reveals that the probability of an instantaneous temperature above 1500°C is small. Hence, it is concluded that thermal- NO_x plays a smaller role in the formation of NO_x in these flames, as compared to the prompt- NO_x .

Fig. 6 shows radial profiles of local mean concentrations of NO_x , UHC and gas temperatures for flames P6 and P8 at five axial locations. As a consequence of the combustion chamber being insulated, flames P6 and P8 present higher temperature levels: the maximum mean temperatures measured for flames P6 and P8 are about 1400 and 1300°C , respectively. These maximum temperatures are

still too low to promote extensive NO_x -thermal formation even considering the turbulent fluctuations. Moreover, as in flames P1 and P4, near the flame axis, the high NO_x and UHC concentrations and the relatively low gas temperatures measured indicate that the prompt mechanism is still an important, if not dominant, source of NO_x in flames P6 and P8.

We have not conducted detailed in-flame data for any of the flames of groups III and IV. As a consequence of the combustion chamber not being insulated (see Table 1) we firmly believe that, once again, NO_x formation was dominated by the prompt mechanism in all of these flames. In conclusion, the flames that have been established present a wide range of NO_x emissions to which the prompt mechanism contributed in a dominant way. Possible exceptions can be flame P6–P12—we shall return to this point in the following subsection.

6.2. Diagnostic system

Photometric images of OH and CH radicals were obtained for all furnace operating conditions included in Table 1 from different flame zones as described in a previous section. The flame zones analysed with the imaging device have been selected according to the in-flame data. Zone 1 (see Fig. 3) has proved to be the most adequate for the purposes of this study not only because it presented the highest intensities of spontaneous emission of the OH and CH radicals but also because exhibited their greatest variations accordingly with the different flames. This suggests that zone 1 controls the NO_x formation/emission in agreement with the in-flame data. In the present article only the photometric data obtained from zone 1 is included.

Figs. 7–9 represent the variation of the NO_x emission, normalised by its maximum, with the OH, CH and OH + CH intensities, each normalised by its maximum value, respectively. The need to normalise the intensity of each radical by its maximum value results from the cathode efficiency wavelength dependence and from the different transmissivity and bandwidth of the filters. In each figure, the solid line represents the best curve-fit—a logarithmic function—obtained using the least-squares approximation. The similar trends of the data plotted in Figs. 7–9 clearly support the choice of the two radicals as indicators of the NO_x formation in the present flames.

In Fig. 7 the correlation of the normalised NO_x emissions with the normalised OH spontaneous emission is relatively poor (correlation factor of 0.83). A systematic deviation from the solid line occurs for flames P6–P12. For these flames the normalised values of OH are all located below the solid line. This appears to confirm the doubts expressed in the end of the previous subsection, i.e. flames P6–P12 present the greatest thermal/prompt formation ratio of all flames that have been studied.

In Fig. 8 the correlation of the normalised NO_x emissions

with the normalised CH spontaneous emission does not present systematic deviations from the solid line for any group of flames being the correlation factor 0.89. This suggests that the NO_x formation in the present flames is dominated by the prompt mechanism as the spontaneous emission of the radical CH is solely associated with this mechanism—reaction (4).

Figs. 7 and 8 suggest that an improved correlation can be obtained by plotting the normalised NO_x emissions with the normalised OH + CH spontaneous emission which is showed in Fig. 9. Indeed an improved correlation is found which can be mathematically expressed through the following function:

$$\frac{\text{NO}_x}{(\text{NO}_x)_{\text{max}}} = 0.26 \ln \left[\frac{\text{OH}}{(\text{OH})_{\text{max}}} + \frac{\text{CH}}{(\text{CH})_{\text{max}}} \right] + 0.74, \quad (9)$$

the correlation factor being 0.94. In spite of this factor being good, surely it could be improved if the relation between the local rates of NO_x formation and the local emission intensities of the two radicals were firmly determined. This is simply impossible to accomplish with the present imaging device owing to the nature of its measurements (line-of-sight measurements). In view of this along with the impossibility to quantify exactly the prompt and thermal contributions for each flame, the degree of success is noteworthy.

The non-intrusive NO_x diagnostic system developed and tested in the present investigation appears to be a powerful tool to control in real time NO_x emissions showing promising features to be applied to a wide range of gas-fired combustion equipment provided that the prompt mechanism is an important route for the NO_x formation. The system is currently being applied to an 0.5 MW pilot furnace firing gas where NO_x is formed mainly via the thermal mechanism.

7. Conclusions

An experimental study has been performed in a small-scale laboratory furnace fired by a propane or ethylene swirl burner to develop and test a NO_x diagnostic system based on a spectral ultraviolet/visible imaging device. The data reported include flue-gas concentrations of O₂, CO₂, CO, UHC and NO_x, and photometric data of spontaneous emission of OH and CH radicals from various regions of the flame. These data have been obtained for twenty three furnace operating conditions which quantify the effects of the gaseous fuel (propane or ethylene), flue-gas recirculation, heat losses through the furnace walls to the surroundings and excess air. The main conclusions drawn from the present results are the following:

1. As a result of the broad furnace operating conditions studied it was possible to obtain a wide range of NO_x emissions. Further, detailed in-flame data of local mean major gas-phase species and gas temperatures collected

- for four furnace operating conditions showed that the NO_x formation is dominated by the prompt mechanism.
2. The results reveal that there is an excellent correlation between the NO_x emissions from propane or ethylene flames and the OH + CH photometric data, which can be mathematically expressed as a logarithmic function, provided that the radical images are collected from a flame zone close to the burner exit.
3. The present non-intrusive NO_x diagnostic system appears to be a powerful tool to control in real time NO_x emissions and shows promising features to be applied to a wide range of gas-fired combustion equipment provided that the prompt mechanism is the dominant route for the NO_x formation.

Acknowledgements

Financial support for this work was partially provided by the European Commission-DGXII (JOULE Programme)—and is acknowledged with gratitude. The authors wish also to thank technicians Manuel Pratas and Vasco Fred for their valuable contributions to the experiments and are grateful for the cooperation of Jorge Coelho during the preparation of the figures.

References

- [1] Nagase K, Funatsu K. SAE Techn. Paper Ser., No. 881226, 1989.
- [2] Nagase K, Funatsu K. SAE Techn. Paper Ser., No. 901615, 1990.
- [3] Block B, Möser P, Hentschel W. Submitted to Optical Engineering.
- [4] Leipertz A, Obertacke R, Wintrich F. Twenty-sixth symposium (International) on combustion, The Combustion Institute, Pittsburgh, PA, 1996:2869–2875.
- [5] Luczak A, Eisenberg S, Knapp M, Schluter H, Beushausen V, Andresen P. Twenty-sixth symposium (International) on combustion, The Combustion Institute, Pittsburgh, PA, 1996:2827–2834.
- [6] Zel'dovich Ya. B, Sadovnikov P Ya, Frank-Kamenetskii D A. Oxidation of nitrogen in combustion, translated by Shelef M, Academy of Sciences of USSR, 1947.
- [7] Miller JA, Bowman CT. Prog Energy Combust Sci 1989;15:287–338.
- [8] Drake MC, Correa SM, Pitz RW, Shyy W, Fenimore CP. Combust Flame 1987;69:347–365.
- [9] De DS. J Inst Energy 1981;54:113–116.
- [10] LaVision 2D-Messtechnik GmbH. FlameStar Instruction Manual. Göttingen, 1993.
- [11] Tourin RH. Spectroscopic gas temperature measurement. Amsterdam: Elsevier, 1966.
- [12] Bach JH, Street PJ, Twamley CS. J Physics E: Scientific Instruments 1970;3:281–286.
- [13] Gaydon AG. The spectroscopy of flames. London: Chapman and Hall, 1974.
- [14] Godridge AM. J Inst Energy 1988;61:38–54.
- [15] Costa M, Ruão M, Carvalho MG. Archivum Combustionis 1996;16:77–86.
- [16] Baltasar J, Carvalho MG, Coelho P, Costa M. Fuel 1997;76:919–929.
- [17] Nimmo W, Hampartsoumian E, Clarke AG, Williams A. Proceedings of the Second European Conference of Industrial Furnaces and Boilers, Algarve (Portugal), 1991.